The impact of Indian Ocean dipole on tropical Indian Ocean surface wave heights in ERA5 and CMIP5 models

Gangiredla Srinivas, P. Remya, B. Praveen Kumar, Anuradha Modi, T. Nair

The impact of Indian Ocean Dipole on tropical Indian Ocean surface wave heights in ERA5 and CMIP5 models

Gangiredla Srinivas[1,2]*, P.G. Remya[1], B. Praveen Kumar[1], Anuradha Modi[1] and T.M. Balakrishnan Nair[1]

[1]Indian National Centre for Ocean Information Services, Hyderabad – 500090, India

[2]LOCEAN-IPSL, Sorbonne Université (UPMC, Univ Paris 06)-CNRS-IRD-MNHN, Paris, France

*E-mail: sgangiredl@locean-ispl.upmc.fr

This article has been accepted for publication and undergone full peer review but has not been through the copyediting, typesetting, pagination and proofreading process which may lead to differences between this version and the Version of Record. Please cite this article as doi: 10.1002/joc.6900

Abstract

The present study examines the relationship between the tropical Indian Ocean (TIO) significant wave height (SWH) and Indian Ocean Dipole (IOD) during boreal summer season (JJA, June through August) in the latest version of ECMWF reanalysis (ERA5) and wave simulations forced with surface winds and sea-ice fields from the Coupled Model Intercomparison Project version-5 (CMIP5) models. The interannual variability of SWH shows a significant negative correlation with the IOD over TIO. SWH anomalies display meridional tripole pattern with significant negative (positive) anomalies over eastern equatorial Indian Ocean caused by anomalous easterlies (westerlies), and positive (negative) anomalies over southeastern TIO and the north Bay of Bengal during positive (negative) phase of IOD. The strong wave heights are noticed along the east coast of India during positive IOD and the south and southwest coast of India during negative IOD. CMIP5 models GFDL-CM3, MRI-CGCM3 and the multi-model mean display considerable skill in capturing these teleconnections with substantial magnitude differences. A thorough understanding of the teleconnections between IOD and TIO wave heights is a significant prerequisite for the accurate forecast of surface waves in the Indian Ocean. Hence, this study advocates the importance evaluating the ability of models in representing the SWH and IOD interactions and its implications on Indian coastal regions in the form of inundation, coastal flooding and other vulnerabilities in a changing climate scenario.

Keywords Significant wave height, Indian Ocean Dipole, Boreal summer season, Surface winds, Tropical Indian Ocean, CMIP5 models

1. Introduction

Indian Ocean (IO) holds unique characteristics among the world oceans due to the seasonal reversal of the monsoon winds and associated ocean dynamic and thermodynamic processes. The Indian summer monsoon (ISM) is one of the most important atmosphere–ocean coupled climate system over the tropics and exhibits substantial variability at seasonal and intraseasonal time scales (Webster *et al.,* 1998). The ISM variability involves changes in the winds over the ocean and hence the ocean surface gravity waves (Shanas and Kumar, 2014). Large ocean waves can be a major hazard for the coastal and offshore operations and activities as they contribute significantly to the coastal sea level extremes and subsequent flooding (Wang *et al.,* 2014). Many previous studies addressed the wave variability, trend and the impact of monsoon winds on the ocean surface waves (Shanas and Kumar, 2014; Anoop *et al.,* 2015; Sanil Kumar and George, 2016). During ISM, high wind sea and swell heights are dominated in the western North Indian Ocean (NIO) because of the strong cross-equatorial Somali jet (Anoop *et al.,* 2015). These monsoon-induced waves are identified as one of the major causes of erosion along the Indian coasts. The Arabian Sea (AS) experiences higher monsoon induced waves compared to the Bay of Bengal (BOB) and hence the

beaches of the west coast of India are more prone to erosion (Chandramohan *et al.,* 1994). At interannual timescales, a significant increasing trend of wave height is seen in the summer monsoon season compared to the post-monsoon in NIO, whereas the pre-monsoon shows a decline in wave heights (Anoop *et al.,* 2015).

The surface wave heights over NIO during boreal summer is mainly associated with the ISM winds. Many previous studies already showed the profound variability of ISM winds from intraseasonal to interannual timescales (Webster *et al.,* 1998; Trenary and Han, 2012; Nagura and McPhaden, 2008). The monsoon circulation is tightly coupled with the variabilities of climate features like the El Nino Southern Oscillation (ENSO), and the Indian Ocean Dipole (IOD) (Saji *et al.,* 1999; Webster *et al.,* 1998; Cherchi and Navarra, 2013). One of the major driving forces at interannual timescales over the tropical Indian Ocean (TIO) is IOD, an intrinsic mode of Indian ocean–atmosphere coupled system (e.g., Saji *et al.,* 1999). An index for IOD, the dipole mode index (DMI) has been defined as the anomalous Sea Surface Temperature (SST) difference between the western Indian Ocean (50-70°E, 10°S-10°N) and the equatorial eastern Indian Ocean (90-110°E, 10°S –equator) (Saji *et al.,* 1999; Webster *et al.,* 1999; Izumo *et al.,* 2010). Previous studies focused on the role of IOD on the wind pattern, and sea level pressure (SLP) variations (Saji *et al.,* 1999; Webster *et al.,* 1999). IOD influences the coastal upwelling over the eastern equatorial Indian Ocean by changing the mean winds (Chen *et al.,* 2016). Anoop *et al.,* (2016) investigated the influence of IOD on the wave climate of the eastern AS during, the peak month of IOD, October. Recently Fu *et al.,* (2018) showed the influence of IOD on surface wave variability with the special emphasis on the Sri Lanka dome region.

The interannual variations in the surface wave heights over the NIO induce strong waves during the monsoon season and affect the marine activities from fishing to coastal management (Chowdhury

and Behera, 2019). In the climate change scenario, investigation of the influence of climate indices on waves received its relevance (Hemer *et al.,* 2012; Anoop *et al.*, 2015; Fu *et al.,* 2018). Since ocean wave information is not simulated in the current general circulation models (GCMs), dynamical and/or statistical downscaling are the useful methods to obtain information about the waves (Morim *et al.,* 2020). Dynamical modelling of ocean waves uses surface winds simulated from the climate model to drive a numerical wave model (Mori *et al.,* 2010; Hemer *et al.,* 2013a; Fan *et al.,* 2014). Hemer *et al.,* (2013b) assessed the projected changes in the ocean surface wave climate at a global scale using a multi-model ensemble from the Coupled Model Intercomparison Project version-5 (CMIP5) models. It is highly computationally demanding and depends heavily on the quality of the surface winds simulated by climate models (Wang *et al.,* 2009). The evaluation of CMIP5 forced wave climate simulations will be beneficial to the research community to identify the processes that control the model skill. Such evaluation is also important to formulate the coastal impacts mitigation strategy and also for better planning and development of coastal and offshore works. But a detailed analysis of IOD influence on TIO surface waves is not yet systematically explored. Therefore, in the present study, we have focused on the impact of IOD on IO surface waves in the latest version of ERA5 reanalysis and wave simulations forced with CMIP5 model wind forcing.

The rest of the paper is organized as follows, section 2 describes the models, data and methodology used for the study. The climatological features of TIO significant wave heights during boreal summer in the wave simulations forced with CMIP5 models outputs are addressed in section 3. The relationship between IOD and TIO surface waves are described in section 4 and summary and conclusions are provided in section 5.

2. Models, data and Methods

We have utilised the wave and wind parameters such as significant wave height (SWH), mean wave period (MWP), mean wave direction (MWD), zonal and meridional wind components at 10 m from the latest version of the European Centre for Medium-Range Weather Forecasts (ECMWF) reanalysis (ERA5) with the horizontal resolution 0.5^{O} x 0.5^{O} during the period 1979 to 2018 for the present study (Hersbach et al., 2020). ERA5 combines the model data with observations from across the world to get a complete and consistent global dataset using the data assimilation techniques. It provides hourly estimates of a large number of atmospheric, land and oceanic climate variables. Naseef and Sanil Kumar (2019) validated the ERA5 reanalysis SWH against in-situ buoy observations and shown that the ERA5 SWH has good agreement with measured buoy data in the IO coastal and deep waters with minimal biases. This study has given us the confidence to proceed with the present analysis using ERA5 wave data. Monthly Sea Surface Temperature (SST) is used from the Extended Reconstructed SST (ERSST) version 4 (Huang *et al.,* 2015). Anomalies are computed based on the climatology of 1979 – 2018 period. Analysis has been carried out by compositing the wave parameters for positive and negative IOD.

Besides, we have used the output from WAVEWATCH III (v3.14) wave model forced with the 3 hourly surface winds and linearly interpolated monthly sea-ice concentration fields from the Coupled Model Intercomparison Project (CMIP5) models for the period 1979-2005 (Hemer *et al.,* 2013b; Hemer and Trenham, 2016). The details of the models used in this study are provided in table 1. Multi-model ensemble (MME) mean is computed by averaging all CMIP5 models outputs. Furthermore, we have also used in-situ wave rider buoy observations located over BOB and AS (Figure 10b) to strengthen our discussion. Six buoys (4 buoys in BOB and 2 buoys in AS) deployed over the NIO are selected in such a way to get long time series for the comparison with model data.

Additional information about the buoy observational network located over NIO is available in Remya *et al.,* 2016.

3. TIO surface wave climatology during boreal summer

The seasonal cycle of surface wind speed (Ws) and significant wave height (SWH) based on the monthly climatology of 40 years (1979-2018) data from the latest version of ECMWF reanalysis (ERA5) over the tropical Indian Ocean (TIO; 40°-110°E and 25°S-25°N), Arabian Sea (AS; 50°-75°E and 0-25°N), Bay of Bengal (BOB; 80°-95°E and 0-20°N) equatorial Indian Ocean (EIO; 40°-110°E and 10°S-10°N) and southern tropical Indian Ocean (STIO; 40°-110°E and 20°S to the equator) are illustrated in Figure 1. Ws display its maximum magnitude during boreal summer months (JJA; June through August) in TIO, AS, BOB, EIO and STIO. The seasonal cycle of Ws shows slightly higher magnitudes over AS compared to other regions (Figure 1a) during JJA. Strong winds over the STIO region are noticed throughout the year with minimal seasonal variability. The seasonal cycle of SWH displays a similar pattern of variability as seen in the Ws with larger heights during JJA (Figure1b). The correlation coefficient between SWH and Ws is found high (~0.91) over AS (Kumar *et al.,* 2013). In STIO, high wave heights are seen throughout the year and it is attributed by the strong south-easterly trade winds persistent there. The wave heights during boreal winter and spring seasons display higher magnitudes over BOB compared to AS. But the surface wind pattern over AS is slightly stronger than the BOB (Figure 1b). This might be due to the SIO swell propagation towards BOB (Zheng *et al.,* 2018). The TIO wave climate shows a large response to seasons and has a maximum wave height during JJA (Chempalayil *et al.,* 2012; Anoop *et al.,* 2015). Therefore, understanding the wave variability during JJA is necessary due to its large implications on Indian coastal regions by inundation, coastal flooding and other

vulnerabilities in the changing climate. Here, we have analysed the mean state of surface wind and wave during boreal summer season (JJA) in ERA5 and CMIP5 models.

The climatology of surface winds for ERA5 and CMIP5 models during JJA are illustrated in Figure 2. The surface winds are strong over AS, STIO, and moderate over BOB and weak over EIO region (Figure 2a). During boreal summer, a strong cross-equatorial flow occurs in the form of a low-level jet with a core speed of 15-25 m/s and with strong horizontal and vertical shears over AS (Joseph and Sijikumar, 2004). All the models have simulated the strong winds over AS, STIO and weak winds over EIO as noticed in reanalysis (Figure 2b-j). ACCESS1.0, BCC-CSM1.1, HaGEM2-ES and MRI-CGCM3 models display stronger winds over BOB unlike in the ERA5. MIROC5 displays strong low-level jet over AS (Figure 2i). Models GFDL-CM3, INMCM4, MRI-CGCM3 and the multi-model mean (MME) display weak winds over AS compared to ERA5. Subsequently, we analysed the impact of these wind differences on mean wave patterns. JJA seasonal mean significant wave height and mean wave direction for ERA5, MME and all individual models are displayed in Figure 3. The climatology of SWH shows wave heights in the range of 1.5- 4 m with a maximum over AS and STIO (Figure 3a). The wave heights over AS are highly influenced by the wind-seas due to the strong fetch and duration caused by southwest monsoon wind flow, rather than the swells that are generated and arriving from the STIO with the southwesterly mean wave direction over AS (Vethamony *et al.*, 2013). Further, moderate wave heights with southerly direction are noticed in the BOB with the range from 2 – 2.5 m. Models can represent these wave maxima as noticed in the ERA5. BCC-CSM1.1, HadGEM2-ES and MRI-CGCM3 display high waves over BOB compared to ERA5. MIROC5 is overestimating wave heights over AS due to the high winds (Figure 3i and 2i). GFDL-CM3, INMCM4, MRI-CGCM3 models and the MME display weaker wave heights over AS due to low winds. Studies comparing the skill of CMIP5 models for

non-standard climate variables, especially the surface wind speed over the ocean, are limited (Hemer and Trenham, 2016). Lee *et al.*, (2013) evaluated the performance of a subset of CMIP3 and CMIP5 models for wind stress over the ocean and stated that CMIP ensemble zonal wind stresses are too weak and result in too small of an east-west gradient of sea level. However, it is important to note that models can represent the mean features of wave heights over NIO, but with considerable magnitude, differences compared to ERA5. Since the wave model output is critically dependent on the choice of wind field product (Kumar *et al.*, 2000; Remya *et al.*, 2014), these differences in wave heights are due to the variations in CMIP5 wind forcing to models. The SWH anomalies display strong interannual variability with wave heights ranging from -2.5 to 2.5m over the EIO during JJA. Interestingly, the interannual variability of SWH is significantly correlated with the Dipole mode index (DMI) with a negative correlation of 0.5 during JJA (Figure 4). The influence of IOD on equatorial IO waves is discussed in the study of Fu *et al.*, (2018). However, this study mainly focused on the Sri Lanka dome region. A detailed investigation of the influence of IOD on tropical Indian Ocean surface wave heights during JJA is very essential in the prospect of offshore industries and coastal vulnerability of the Indian Ocean rim countries especially Indian coastal regions as it is severely affected by strong monsoonal waves. Furthermore, the prediction of ocean state in a changing climate is very crucial for marine activities. This motivated us to study the impact of IOD on TIO SWH in the wave simulations from the historical runs of the CMIP5 models. The IOD events are identified if the normalised SST anomaly difference between Western Equatorial Indian Ocean (WEIO; 50-70ºE and 10ºS-10ºN) and Eastern Equatorial Indian Ocean (EEIO; 90-110ºE and 10ºS to the equator) exceed one standard deviation during JJA are considered for analysis. Based on the above criteria, we got the following events for positive IOD (1983, 1987,

1991, 2012, 2015 and 2017) and negative IOD cases (1985, 1989, 1992, 1996, 2001, 2013 and 2016). Detailed analysis is carried out for the composites of positive and negative IOD events.

4. The relationship between IOD and TIO SWH in ERA5 and CMIP5 models

The composites of SWH and surface wind anomalies for ERA5 and CMIP5 models during pIOD and nIOD years are illustrated in figures 5 and 6 respectively. The SWH anomalies display a meridional tripole pattern with significant negative anomalies (red square) over Eastern EIO and positive anomalies over south-eastern TIO and north BOB regions (black squares) during pIOD years (Figure 5a-j). Surface winds display the strong easterly wind anomalies from south-eastern AS to eastern EIO region (Figure 6a). This pattern of wind is due to the low pressure in the western equatorial IO due to the warm water in this region compared to the eastern equatorial IO (Vinayachandran *et al.,* 2009). The anticyclonic wind anomalies are seen over BOB and southeast TIO as a response to positive IOD conditions. During pIOD, correspond to the warm SST anomaly over western EIO, there is an anomalous atmospheric low-level convergence. In contrast, anomalous low-level divergence (anticyclonic circulation) forms over the regions east of 90ºE and west of Sumatra and north BOB induced by the cold SST anomaly (Qiu *et al.,* 2014) and vice-versa during nIOD. These anomalous anticyclonic circulations on either side of the equator and strong easterlies on the equator are responsible for the SWH tripole pattern anomalies over eastern EIO (Figure 6a). SWH anomalies are significantly negative over eastern EIO where IOD induced easterlies act on the mean state westerlies. Besides, the mean wave period (MWP) anomaly composite for ERA5 and CMIP5 models during pIOD years show positive MWP anomalies over the eastern EIO and intensified negative wave period anomalies over the south-eastern TIO region (Figure 7a-j). The weak positive anomaly of wave period in the eastern EIO indicates the dominance of swell during positive IOD years (Figure 7a). The weak westerly winds slow down the

wave growth in the eastern EIO. Reduction in the wind sea generation in the area creates a significant negative anomaly in the SWH and a positive anomaly in the wave period. Similarly, in the BOB and Eastern TIO, IOD wind anomalies positively impact the mean state and increase the wave growth in these regions. The increased wave growth is indicated by a positive anomaly in the SWH and a negative anomaly in the MWP (Figure 7a and 5a). By analysing the MWP anomalies in the EIO, it is seen that positive IOD has a negative influence on the equatorial wind-wave generation. However, none of the models could represent the meridional tripole pattern as seen in the reanalysis (Figure 5). GFDL-CM3, MRI-CGCM3 and the MME display tripole pattern with weaker magnitudes and shift in the positive and negative anomalies (Figure 5b, 5f and 5j). These models and the MME display easterly wind anomalies over eastern EIO driven by the IOD conditions (Figure 6b, 6f and 6j). They display anticyclonic circulation anomalies over north BOB and south-eastern TIO region as seen in the ERA5. ACCESS1.0, BCC-CSM1.1, GFDL-CM3, MIROC5 and MRI-CGCM3 capture the easterly wind anomalies over eastern EIO but fails to represent the negative SWH anomalies over eastern EIO (Figure 6 and 5). GFDL-CM3 and MRI-CGCM3 models display similar tripole pattern in MWP anomalies as seen in the ERA5 (Figure 7b, 7f and 7j). Rest of the models display inconsistent MWP anomalies as not seen in the ERA5. Even though many CMIP5 (for example ACCESS1.0, BCC-CSM1.1, GFDL-CM3, MIROC5, MRI-CGCM3) models and the MME reproduced the easterly wind anomaly patterns fairly well, they failed to similarly reproduce the SWH and MWP.

The composites of SWH and surface wind anomalies during nIOD years for ERA5 and CMIP5 models (Figure 5k-t and 6k-t) also show meridional tripole pattern with negative SWH anomalies over south-eastern TIO and north BOB (red square), and significant positive SWH anomalies over eastern EIO (black square) during JJA (Figure 5k). The observed meridional tripole pattern during

the nIOD years is exactly opposite to the pIOD years with strong wave heights over EIO (Figure 5a and 5k). However, the impact of nIOD on coastal regions of India is different from the pIOD. The westerly wind anomaly along the equator is a distinct feature of the nIOD years. The composite of surface wind displays westerly wind anomalies over the central EIO and negative anomalies with anomalous cyclonic circulation over BOB and eastern TIO (Figure 6k). The eastern IO, which comprises of eastern EIO, south-eastern TIO and north BOB regions, clearly show a tripole pattern opposite to the pIOD pattern in the wind. The MWP anomalies are positive over BOB and south-eastern TIO during the nIOD events indicating a reduction in the wind sea generation (Figure 7k). The weak negative MWP anomalies over the south of the India landmass indicates that the SWH anomalies are generated due to wind-seas. The turbulent sea state generated by the dominance of short-period waves over western coastal regions of India during the nIOD leads to enhanced wave heights over there. Importantly, during the nIOD years south-western and southern coastal regions of India experiences the anomalous strong wave heights in JJA. Usually, the southwest coastal regions and southern tip of India experience high wave activity (mean SWH of ~2m) during monsoon and the coastal population is severely affected by erosion and flooding. During nIOD, enhanced wave activity over the AS will have an adverse impact on the western coastal areas. Other areas like BOB, east coast of India and offshore and coastal areas of north-eastern AS experience low wave activity compared to normal years during JJA. However, the tripole pattern seen in the ERA5 is not reproduced by CMIP5 models except MRI-CGCM3, GFDL-CM3 and the MME with considerable differences in the magnitude (Figure 5l and 5t). CNRM-CM5 display positive SWH anomalies over northern Arabian Sea and Bay of Bengal unlike in the ERA5 (Figure 6o). This may be due to the improper representation of IOD winds which is driven by the weaker SST gradients during the negative IOD events (Figure 8o). GFDL-CM3, MRI-CGCM3 and the MME display a

similar pattern of MWP anomalies as noticed in the ERA5. CNRM-CM5 and HadGEM2-ES show negative MWP anomalies in most of the TIO region. MIROC5 display positive MWP anomalies over most of the regions (Figure 7s). Therefore, the TIO SWH anomalies during JJA are largely modulated by the IOD at interannual time scales. Besides, to strengthen our discussion we have used the in-situ wave rider buoy observations located over BOB and AS (Fig. 10b) for the analysis. The composite of pIOD years during JJA suggested that the eastern AS experiences a reduction in the wave height whereas BOB gets high wave activity during pIOD (Figure 10a). Conversely, the composites of nIOD years showed a marginal increase in the sea height over AS, whereas a decrease in the sea height is seen over BOB (Figure 10a). Further analysis of the observational evidence of IOD influence on waves is limited due to the lack of continuous data and more observation points.

The influence of IOD on the SWH mainly depends on the modification of the wind field caused by the phases of the IOD event (Anoop *et al.,* 2016; Fu *et al.,* 2018). If this wind pattern is absent even during a strong IOD event, then the signature of the IOD on the SWH is also absent. This alteration of wind pattern mainly depends on the IOD induced SST variability in the eastern and western EIO. The composites of SST anomalies for pIOD and nIOD years for ERA5 and as well as CMIP5 models during JJA are displayed in figure 8. A distinct feature of the pIOD is a well-established east-west dipole pattern with significant positive SST anomalies over WEIO and negative SST anomalies over EEIO (Figure 8a). A very weak negative SST anomaly pattern over north BOB is also noticed. The CMIP5 models have captured the east-west dipole pattern with warm SST anomalies over WEIO and cold SST anomalies over EEIO as seen in the ERA5. Models ACCESS1.0, GFDL-CM3, INMCM4, MRI-CGCM3 and the MME show good skill in representing the SST anomalies over EEIO during pIOD years. These models display weak SST anomaly

gradients with spatial drift unlike in the ERA5. BCC-CSM1.1, CNRM-CM5, HadGEM2-ES and MIROC5 displayed EEIO cold SST anomalies and failed to capture the positive SST anomalies over WEIO during pIOD events. MIROC5 display abnormal warming pattern in the central EIO unlike in the ERA5 (Figure 8i). The composites of SST anomalies during the nIOD years display an east-west gradient with negative SST anomalies over WEIO and positive SST anomalies over EEIO (Figure 8k). The cold SST anomalies over WEIO and warm SST anomalies over EEIO during the nIOD years are captured by the 3 models (BCC-CSM1.1, GFDL-CM3 and MRI-CGCM3) and the MME with the considerable skill. ACCESS1.1 and HadGEM2-ES display strong WEIO cooling compared to other models. CNRM-CM5 show the EEIO warming extended to the central EIO unlike in the ERA5 (Figure 8o). MIROC5 display WEIO cold SST anomalies shift to central STIO region which is not seen in the ERA5. Also, the correlation analysis between ERA5 and CMIP5 models display a significant correlation in models GFDL-CM3, HadGEM2-ES, MIROC, MRI-CGCM3 and also with MME (Figure not shown). These models are described as the best models for IOD in terms of the correlation coefficient pattern between observations and simulations (Chu *et al.*, 2013). Furthermore, it is noted that these models also showed good skill in capturing the teleconnection between TIO SWH and IOD. The discrepancy in accurately simulating the IOD in CMIP5 models is due to improper representation in Bjerkness feedback in the equatorial Indian Ocean involving winds, SST and thermocline leading to the biases/errors (Cai and Cowan, 2013). The above analysis suggests that the disparities seen in the winds from different models are due to the discrepancy in the IOD SST anomalies.

In addition, the predictability skill of CMIP5 models in representing the teleconnection between IOD and SWH anomalies is further explained through the correlation coefficient (CC) analysis displayed in figure 9. The CC between DMI and TIO SWH anomalies in ERA5 is negatively

correlated with a value -0.48 (significant with 90% confidence level). GFDL-CM3, MRI-CGCM3 and the MME displayed good skill in capturing the teleconnection between IOD and SWH anomalies both in pIOD and nIOD conditions. The negative CC between DMI and SWH displayed in these models as seen in the ERA5. BCC-CSM1.1, CNRM-CM5 and MIROC5 models also display a negative correlation between DMI and SWH. However, the composite analysis of SWH and pIOD, and nIOD years display poor skill in these models. HadGEM2-ES and INMCM4 display the significant positive correlation between DMI and SWH anomalies hence the results of SWH composite analyses during pIOD/ nIOD events were poor. Models GFDL-CM3, MRI-CGCM3 and the MME show good skill in reproducing the wave heights due to proper representation of wind anomalies driven by the IOD conditions. Other models failed to reproduce the proper wave heights which are observed in the ERA5 due to the misrepresentation of wind anomalies. Further, these models also had weak skill in reproducing the IOD SST anomalies. Overall analysis suggests that the establishment of teleconnection between SWH anomalies and IOD years depends on the proper representation of surface wind driven by the large-scale air-sea interaction processes in the models.

5. Summary and discussions

The present study examined the relationship between IOD and SWH during boreal summer season (June through August, JJA) over the tropical Indian Ocean using the latest version ECMWF reanalysis (ERA5) and wave simulations forced with the coupled model intercomparison project version-5 (CMIP5) models wind forcing. The seasonal cycle of surface winds and significant wave heights (SWH) displays its maximum variability during JJA over the regions of TIO, AS, BOB, EIO and STIO. The SWH anomalies displayed strong interannual variability during JJA over TIO and this interannual variability in SWH anomalies is negatively correlated with the Dipole Mode Index (DMI) with the value of ~0.5 (Saji *et al.*, 1999; Anoop *et al.*, 2016, Fu *et al.*, 2018). The

composites of SWH anomalies displayed a meridional tripole pattern with positive SWH anomalies over north BOB, south-eastern TIO and significant negative SWH anomalies over eastern EIO during the positive IOD (pIOD) years and vice-versa during the negative IOD (nIOD) years. The negative SWH anomalies seen over eastern EIO are due to the easterly anomalies act on the mean westerlies and positive anomalies are seen over the southeastern TIO and BOB where the wind anomalies enhanced the mean wind fields. Therefore, during pIOD years, BOB, east coast of India and offshore and coastal areas of northeastern AS experience more wave activity compared to normal years during JJA (Kumar *et al.*, 2019). BOB has a mean wave height ~3m during JJA and a significant positive increase of SWH during pIOD will create rougher sea conditions in the eastern coastal areas of India. On the other hand, southwest coastal regions and the southern tip of India experience less wave activity during monsoon in a pIOD year. Similarly, during nIOD events, the composites of SWH anomalies shows strong positive anomalies with westerly wind anomalies over EIO. The positive SWH anomalies during nIOD intensify the wave activity over the southwest and southern coastal regions and may adversely affect the coastal regions. Accurate wave forecast during JJA with an IOD would be a great advantage for the fisheries community and offshore marine activities to prevent damages due to the high wave heights over the tropical Indian Ocean. The models GFDL-CM3, MRI-CGCM3 and the MME displayed good skill in representing the meridional tripole pattern of SWH anomalies due to the appropriate wind forcing driven by the SST anomalies during the IOD years. Rest of the models displayed poor skill in representing these wave anomalies due to the discrepancy in the wind forcing. Thus, this study advocates that the proper representation of teleconnection between IOD and SWH in CMIP5 models can be attained through the improvement of the CMIP5 model wind forcing in interannual time scales by representing the large-scale air-sea interaction processes accurately.

Acknowledgement

We thank Director, ESSO-INCOIS for support. We thank Dr. Mark Hemer, Principal Research Scientist, Sea-Level, Waves and Coastal Extremes, Team Leader Climate Science Centre, CSIRO Oceans & Atmosphere, Australia for providing the Coupled Model Intercomparison Project (CMIP5) model simulations. We thank Dr. Jasti S. Chowdary, Scientist, ESSO-IITM for his support and help in discussions. Details are available in https://cowclip.org/data-access. The latest version of ECMWF reanalysis (ERA5) dataset can be accessible at https://cds.climate.copernicus.eu/cdsapp#!/dataset/reanalysis-era5-single-levels?tab=form. Figures are prepared in PyFerret. This is INCOIS contribution number XYZ.

ORCID

Gangiredla Srinivas https://orcid.org/0000-0002-8649-5846

References

Anoop, T.R., Sanil Kumar, V., Shanas, P.R., and Johnson, G. (2015) Surface wave climatology and its variability in the North Indian Ocean based on ERA-Interim reanalysis, *Journal of Atmosphere Ocean Technology*, 32:1372–1385. doi:10.1175/JTECH-D-14-00212.1.

Anoop, T.R., Sanil Kumar, V., Shanas, P.R., Glejin, J., and Amrutha, M.M. (2016) Indian Ocean Dipole modulated wave climate of eastern Arabian Sea, *Ocean Sciences*, 12:369–378. doi:10.5194/os12-369-2016.

Chandramohan, P., Nayak, B.U., Sanil Kumar, V., and Pathak, K.C. (1994) Beach processes between Mulgund and Shiroda, west coast of India, *Indian Journal of Marine Sciences*, 23:102–104.

Chempalayil, P., Sanil Kumar, V., Glejin, J., Udhaba, D.G., and Vinayaraj, P. (2012) Interannual and seasonal variations in nearshore wave characteristics off Honnavar, west coast of India, *Current Science*, 103:286–292.

Chen, G.D., Han, W.Q., Li, Y.L., and Wang, D.X. (2016) Interannual variability of equatorial eastern Indian Ocean upwelling: local versus remote forcing, *Journal of Physical Oceanography*, 46:789–807. https://doi.org/10.1175/JPO-D-15-0117.1.

Cherchi, A, and Navarra, A. (2013) Influence of ENSO and of the Indian Ocean dipole on the Indian summer monsoon variability, *Climate Dynamics*, 41:81–103. doi:10.1007/s00382-012-1602-y.

Chowdhury, P., and Behera, M.R. (2019) Evaluation of CMIP5 and CORDEX derived wave climate in Indian Ocean, *Climate Dynamics*, 52:4463. https://doi.org/10.1007/s00382-018-4391-0.

Chu J-E , Ha K-J, Lee J-Y , Wang B, Kim B-H , Chung C. 2013. Future change of the Indian Ocean basin-wide and dipole modes in the CMIP5 . *Climate Dynamics*, 1–17, DOI: 10.1007/s00382-013- 2002- 7

Fan, Y., Lin, S.J., Held, I., Yu, Z., and Tolman, H. (2014) Global Ocean Surface Wave simulation using a coupled atmosphere–wave model, *Journal of Climate*, 25:6233–6252. http://dx.doi.org/10.1175/JCLI-D-11-00621.1.

Fu, C., Wang, D., Yang, L., Yao, L., Zhou, F., Priyadarshana, T., and Yao, J. (2018) The relationship between significant wave height and Indian Ocean Dipole in the equatorial North Indian Ocean, *Ocean Dynamics*, 68:10.1007/s10236-018-1154-8.

Hemer, M.A., and Trenham, C.E. (2016) Evaluation of a CMIP5 derived dynamical global wind wave climate model ensemble, *Ocean Modelling*, 103:190–203. doi:10.1016/j.ocemod.2015.10.009.

Hemer, M.A., Fan, Y., Mori, N., Semedo, A., and Wang, X. L. (2013b) Projected changes wave climate from a multi-model ensemble, *Nature Climate Change*, 3:471–476.

Hemer, M.A., Katzfey, J., and Trenham, C.E. (2013a) Global dynamical projections of surface ocean wave climate for a future high greenhouse gas emission scenario, *Ocean Modelling*, 70:221–245.

Hemer, M.A., Wang, X.L., Weisse, R., and Swail, V.R. (2012) Advancing wind-waves climate science, *Bulletin of American Meteorological Society,* 791-796. doi: 10.1175/BAMS-D11-00184.1

Hersbach, H., Bell, B., Berrisford, P (2020) The ERA5 global reanalysis, *QJ R Meteorological Society* 1-51

Huang, B., Banzon, V.F., Freeman, E., Lawrimore, J., Liu, W., Peterson, T.C., Smith, T.M., Thorne, P.W., Woodruff, S.D., and Zhang, H.M. (2015) Extended reconstructed sea surface temperature version 4 (ERSSTv4) Part I: Upgrades and intercomparisons. *Journal of Climate,* 28(3):911–930

Izumo, T., Vialard, J., Lengaigne, M., de Boyer Montegut, C., Behera, S.K., Luo, J.J., Cravatte, S., Masson, S., and Yamagata, T. (2010) Influence of the state of the Indian Ocean Dipole on the following year's El Niño, *Nature Geoscience,* 3:168–172. doi:10.1038/ngeo760

Joseph, P.V., and Sijikumar, S. (2004) Intraseasonal variability of the low-level jet stream of the Asian summer monsoon, *Journal of Climate*, 17, 1449–1458, doi:10.1175/1520-0442(2004)017<1449:IVOTLJ>2.0.CO;2.

Kumar, D., Sannasiraj, S.A., Sundar, V., and Polnikov, V.G. (2013) Wind Wave Characteristics and Climate Variability in the Indian Ocean Region Using Altimeter Data, *Marine Geodise,* 36: 303-313.

Kumar, P., Kaur, S., Weller, E., Min, S.K., (2019) Influence of Natural Climate Variability on the Extreme Ocean Surface Wave Heights Over the Indian Ocean. *Journal of Geophysical Research (Ocean),* 124, 6176-6199. https://doi.org/10.1029/2019JC015391.

Kumar, R. *et al*., (2000) Ocean wave model sensitivity experiments, Preprints, In Proceedings of the Fifth Pacific Ocean remote sensing Conference (PORSEC), Goa, India, 801–803.

Lee, T., Waliser, D.E., Li, J.L.F., Landerer, F.W., and Gierach M.M. (2013) Evaluation of CMIP3 and CMIP5 wind stress climatology using satellite measurements and atmospheric reanalysis products, *Journal of Climate*, 26:5810-5826.

Mori, N., Yasuda, T., Mase, H., Tom, T., and Oku, Y. (2010) Projection of extreme wave climate change under the global warming, *Hydrological Research Letters* 4:15-19. 10.3178/hrl.4.15

Morim, J. *et al*., (2020) A global ensemble of ocean wave climate projections from CMIP5-driven models. *Scientific. Data* **7**, 105.

Nagura, M., and McPhaden, M.J. (2008) The dynamics of zonal current variations in the central equatorial Indian Ocean. *Geophysical Research Letters,* 35:L23603. doi: 10.1029/2008/GL035961

Naseef Muhammed, Sanil Kumar, T.V. (2019) Climatology and trends of the Indian Ocean surface waves based on 39‐ year long ERA5 reanalysis data. *International Journal of Climatology*, doi:https://doi.org/10.1002/joc.6251

Qiu Y, Cai W, Guo X, Benjamin N. (2014) The asymmetric influence of the positive and negative IOD events on China's rainfall. *Scientific Reports,* 4: 4943, doi: 10.1038/srep04943

Remya, P.G., Kumar, R., and Sujit, B. (2014) An assessment of wind forcing impact on a spectral wave model for the Indian Ocean, *Journal of Earth System Science,* 123:1075-1087.

Remya, P.G., Vishnu, S., Praveen Kumar, B., Balakrishnan Nair, T.M. and Rohith, B. (2016) Teleconnection between the North Indian Ocean high swell events and meteorological conditions over the southern Indian Ocean. *Journal of Geophysical Research, Oceans*, **121**(10), 7476–7494.

Saji, N.H., Goswami, B.N., Vinayachandran, P.N., and Yamagata, T. (1999) A dipole mode in the tropical Indian Ocean, *Nature* 401:360– 363.

Sanil Kumar, V., and George, J. (2016) Influence of Indian summer monsoon variability on the nearshore waves in the eastern Arabian Sea, *Annales de Geophysique* 34:871–885.

Shanas, P.R. and Sanil Kumar, V. (2014) Temporal variations in the wind and wave climate at a location in the eastern Arabian Sea based on ERA-Interim reanalysis data, *Natural Hazards Earth System Science*, 14:1371–1381. doi:10.5194/nhess-14-1371-2014

Trenary, L.L., and Han, W. (2012) Intraseasonal-to-interannual variability of south Indian ocean sea level and thermocline: remote versus local forcing. *Journal of Physical Oceanography*, 42:602–627. doi: 10.1175/JPO-D-11-084.1

Vethamony P, Rashmi R, Samiksha SV, Aboobacker VM (2013) Recent studies on wind seas and swells in the Indian Ocean: a review, *International Journal of Ocean and Climate System*, 4(1):63–73.

Vinayachandran, P.N., Francis, P.A., and Rao, S.A. (2009) Indian Ocean dipole: processes and impacts, Current Trends in Science, Platinum Jubilee Special, Indian Academy of Sciences Bangalore 569-589.

Wang, X.L, Feng, Y., and Swail, V.R. (2014) Changes in global ocean wave heights as projected using multimodel CMIP5 simulations, *Geophysical Research Letters*, 41:1026–1034.

Wang, X.L., Swail, V.R., and Cox, A. (2009) Dynamical versus statistical downscaling methods for ocean wave heights, *International Journal of Climatology*, 30:317–332. doi:10.1002/joc.1899

Webster, P.J., Magaña, V.O., Palmer, T.N., Shukla, J., Tomas, R.A., Yanai, M., and Yasunari, T. (1998) Monsoons: Processes, predictability, and the prospects for prediction, *Journal of Geophysical Research*, 103:14451–14510. doi:10.1029/97JC02719

Webster, P.J., Moore, A.M., Loschnigg, J.P., and Leben, R.R. (1999) The great Indian Ocean warming of 1997–1998: Evidence of coupled oceanic-atmospheric instabilities, *Nature* 401:356–360.

Weller E, Cai W (2013) Realism of the Indian Ocean dipole in CMIP5 models: The implications for climate projections, *Journal of Climate*, 26, 6649– 6659

Zheng, C.W, Li, C.Y., and Pan, J. (2018) Propagation route and speed of swell in the Indian Ocean, *Journal of Geophysical Research (Oceans)*, 123:8–21. https://doi.org/10.1002/2016JC012585

Figure captions

FIGURE 1. The climatological seasonal cycle of a) surface wind speed (m/s) and b) significant wave height (m) over the regions of the tropical Indian Ocean (black line, TIO; 40°-110°E and 25°S-25°N), Arabian Sea (red line, AS; 50°-75°E and 0-25°N), Bay of Bengal (green line, BOB; 80°-95°E and 0-20°N) Equatorial Indian Ocean (blue line, EIO; 40°-110°E and 10°S-10°N) and southern tropical Indian Ocean (magenta line, STIO; 40°-110°E and 20°S to the equator).

FIGURE 2. JJA seasonal climatology of surface wind speed (shaded; m/s) and direction (vector; m/s) for a) ERA5, b) MME, c) ACCESS1.0, d) BCC_CSM1.1, e) CNRM-CM5, f) GFDL-CM3, g) HadGEM2-ES, h) INMCM4, i) MIROC5 and j) MRI-CGCM3.

FIGURE 3. JJA seasonal climatology of significant wave height (shaded; m) and mean wave direction (vectors; m/s) for a) ERA5, b) MME, c) ACCESS1.0, d) BCC_CSM1.1, e) CNRM-CM5, f) GFDL-CM3, g) HadGEM2-ES, h) INMCM4, i) MIROC5 and j) MRI-CGCM3.

FIGURE 4. Time series of JJA seasonal anomalies of TIO significant wave height (m) (black line; m) and Indian Ocean Dipole mode index (red line, DMI).

FIGURE 5. JJA composite anomalies of significant wave height (shaded, m) for (a) – (j) positive and (k) – (t) negative IOD years for ERA5, MME, ACCESS1.0, BCC_CSM1.1, CNRM-CM5, GFDL-CM3, HadGEM2-ES, INMCM4, MIROC5 and MRI-CGCM3 respectively. The green colour stars on the panel a and k shows the buoy locations. Stippling indicates the significance at 90% confidence level.

FIGURE 6. JJA composites of surface wind (shaded and vectors, m/s) anomalies for (a) – (j) positive and (k) – (t) negative IOD years for ERA5, MME, ACCESS1.0, BCC_CSM1.1, CNRM-

CM5, GFDL-CM3, HadGEM2-ES, INMCM4, MIROC5 and MRI-CGCM3 respectively. Stippling indicates the significance at 90% confidence level.

FIGURE 7. JJA composites of mean wave period (shaded, s) anomalies for (a) – (j) positive and (k) – (t) negative IOD years for ERA5, MME, ACCESS1.0, BCC_CSM1.1, CNRM-CM5, GFDL-CM3, HadGEM2-ES, INMCM4, MIROC5 and MRI-CGCM3 respectively. Stippling indicates the significance at 90% confidence level.

FIGURE 8. JJA composites of sea surface temperature (SST, deg C) anomalies for (a) – (j) positive and (k) – (t) negative IOD years for ERA5, MME, ACCESS1.0, BCC_CSM1.1, CNRM-CM5, GFDL-CM3, HadGEM2-ES, INMCM4, MIROC5 and MRI-CGCM3 respectively. Stippling indicates the significance at 90% confidence level.

FIGURE 9. The correlation coefficient between DMI and TIO SWH anomalies during JJA.

FIGURE 10 a) JJA composites of mean wind sea height for normal (blue bar), pIOD (brown) and nIOD (olive green) years. b) locations of considered buoys.

Table 1. Details of CMIP5 models used in this study.

S.No	Model acronym	Modelling centre	Country
1	ACCESS1.0	Commonwealth Scientific and Industrial Research Organization (CSIRO) and Bureau of Meteorology(BOM)	Australia
2	CNRM-CM5	Centre National de Recherches Meteorologiques Centre Europeen de Recherche et Formation Avancees en Calcul Scientifique	France
3	HadGEM2-ES	National Institute of Meteorological Research/Korea Meteorological Administration	Korea
4	INMCM4	Institute of Numerical Mathematics	Russia
5	BCC-CSM1.1	Beijing Climate Center	China
6	MIROC5	Japan Agency for Marine-Earth Science and	Japan

		Technology	
7	GFDL-CM3	National Oceanic and Atmospheric Administration (NOAA)/Geophysical Fluid Dynamics Laboratory (GFDL),	USA
8	MRI-CGCM3	Meteorological Research Institute	Japan

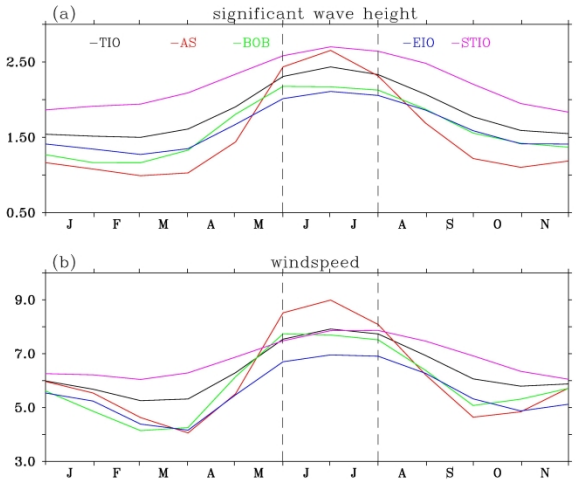

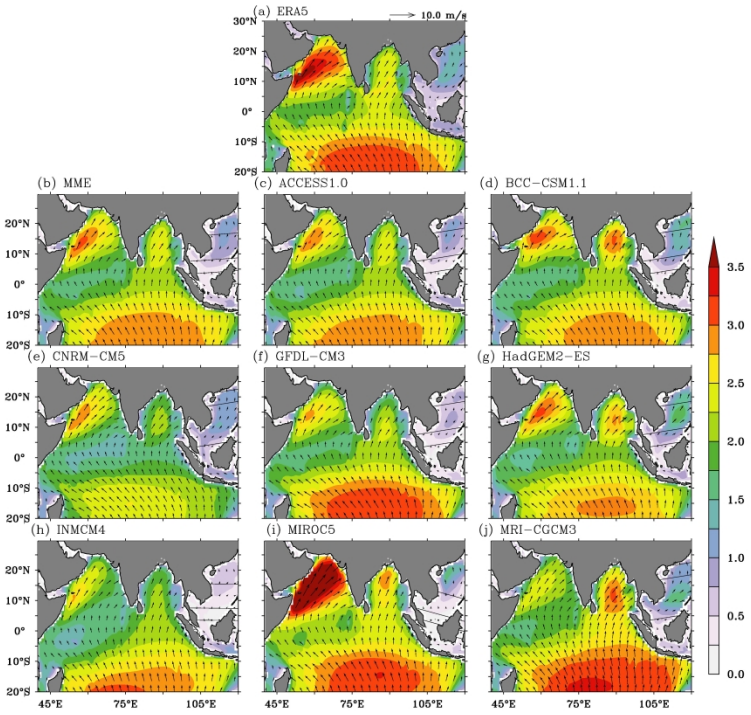

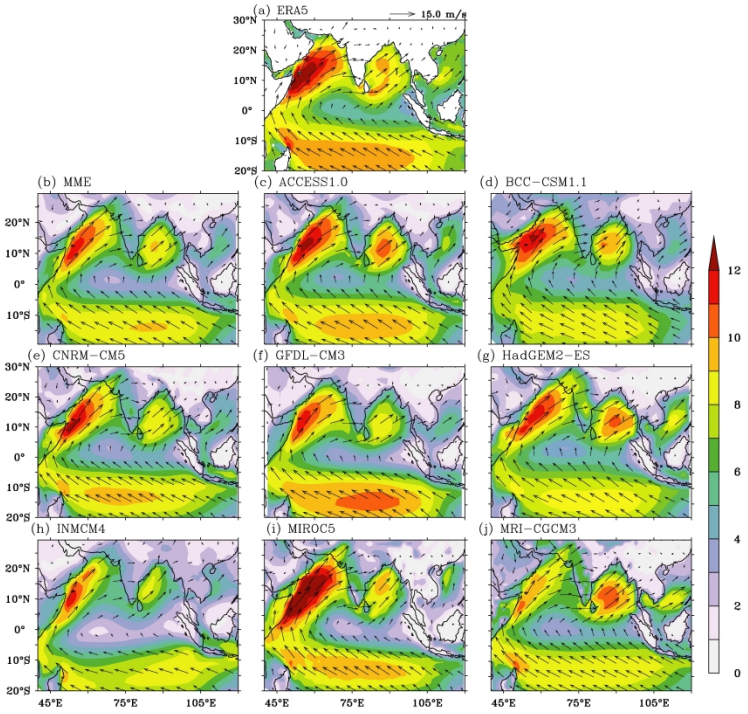

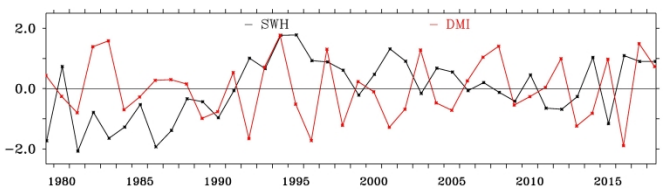

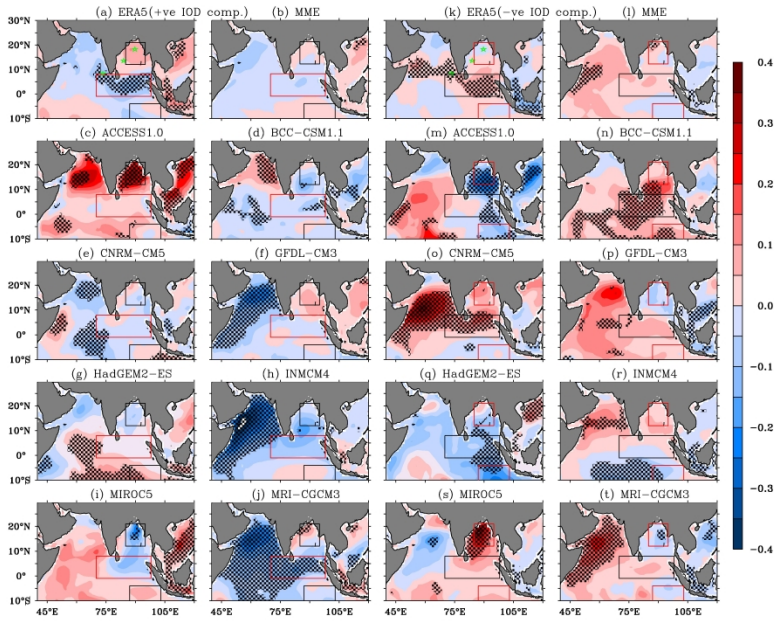

FIGURE 5. JJA composite anomalies of significant wave height (shaded, m) for (a) – (j) positive and (k) – (t) negative IOD years for ERA5, MME, ACCESS1.0, BCC_CSM1.1, CNRM-CM5, GFDL-CM3, HadGEM2-ES, INMCM4, MIROC5 and MRI-CGCM3 respectively. The green colour stars on the panel a and k shows the buoy locations. Stippling indicates the significance at 90% confidence level.

215x279mm (600 x 600 DPI)

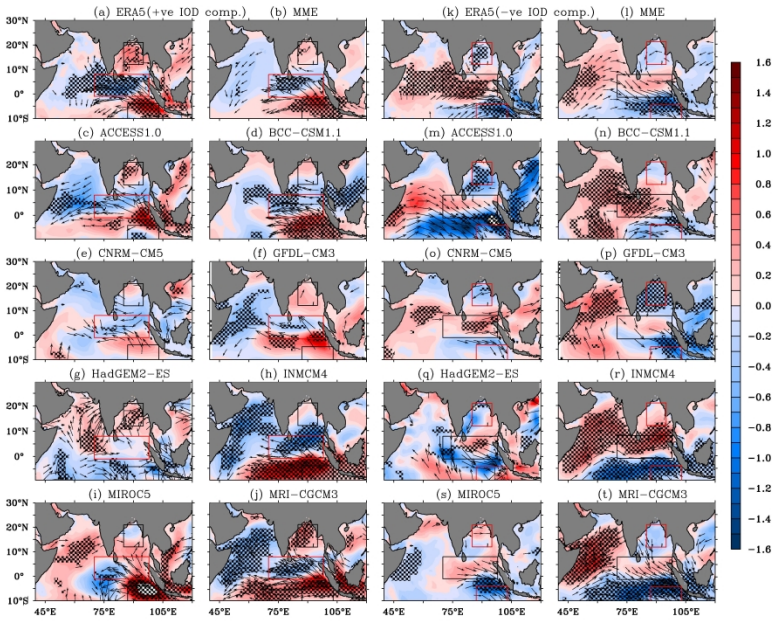

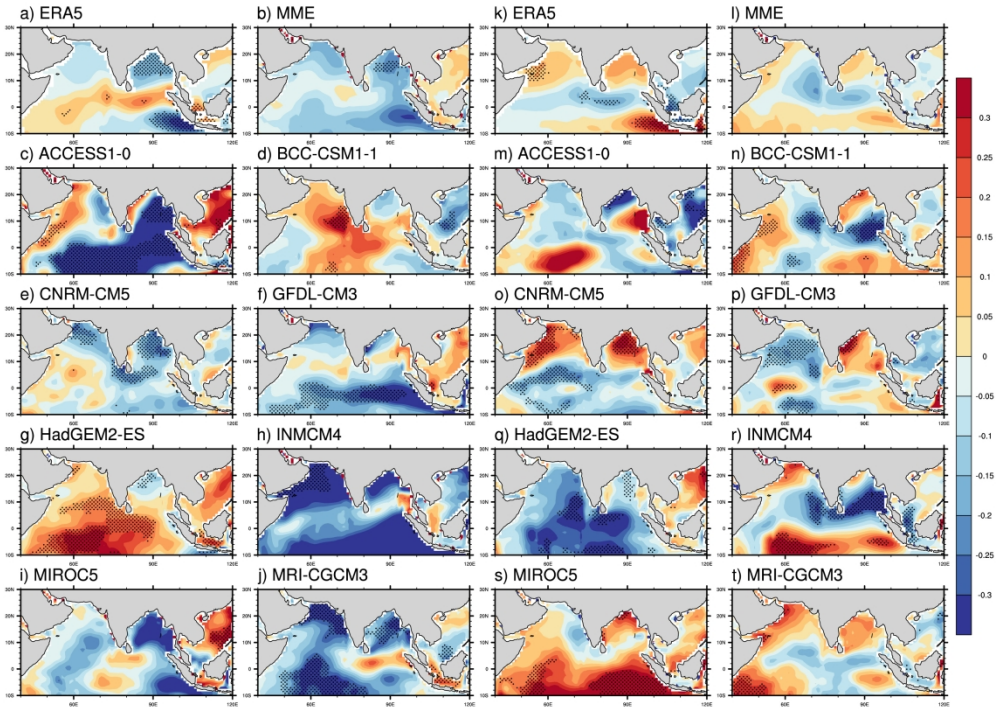

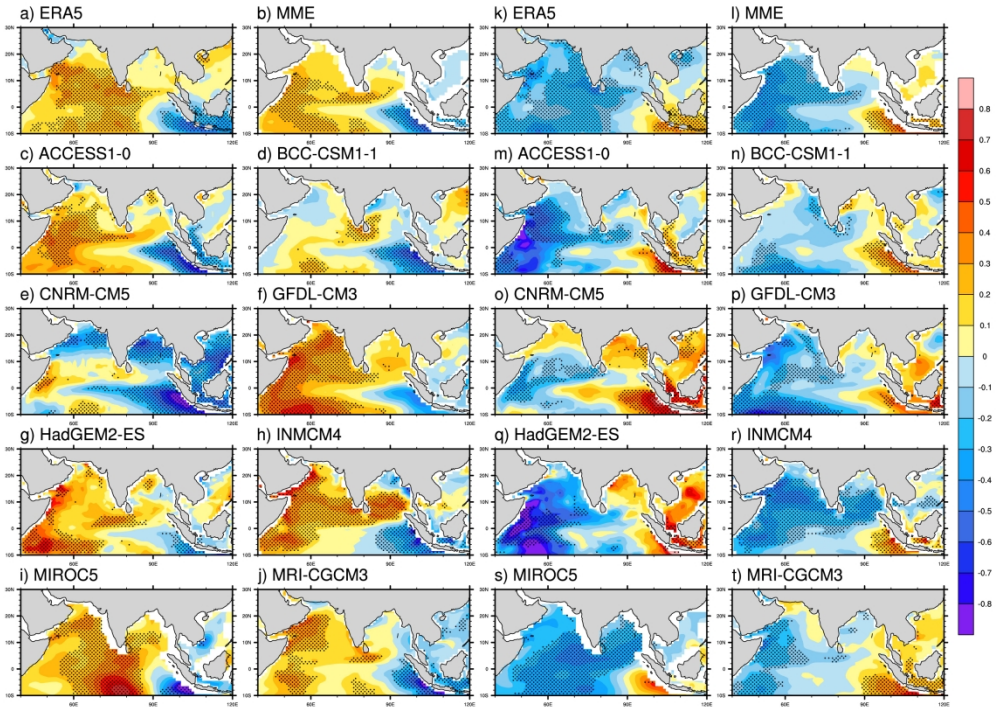

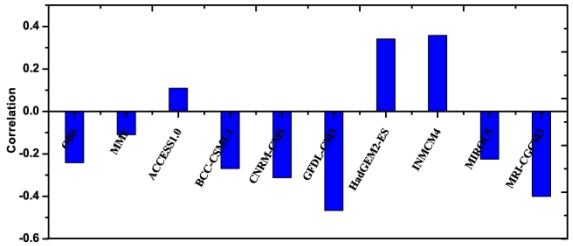

(a)

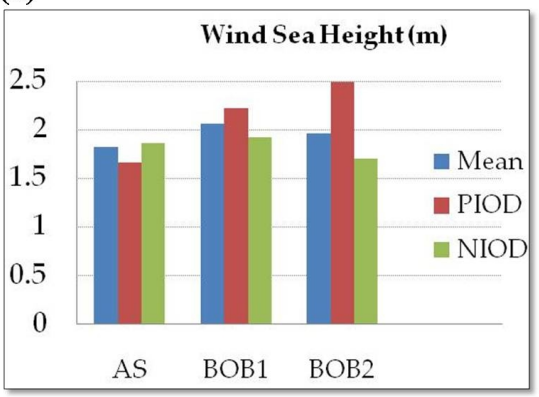

(b)